

## Article

# Effects of Surface Morphology on Erosion–Corrosion and Corrosion Resistance of Highly Hydrophobic Nickel-Tungsten Electrodeposited Film

Parinaz Salehikahrizangi <sup>1,\*</sup>, Keyvan Raeissi <sup>1</sup>, Fathallah Karimzadeh <sup>1</sup>, Luigi Calabrese <sup>2</sup> and Edoardo Proverbio <sup>2</sup>

<sup>1</sup> Department of Materials Engineering, Isfahan University of Technology, Isfahan 84156-83111, Iran; k\_raeissi@cc.iut.ac.ir (K.R.); karimzadeh\_f@cc.iut.ac.ir (F.K.)

<sup>2</sup> Department of Engineering, University of Messina, Contrada di DioSant'Agata, 98166 Messina, Italy; lcalabrese@unime.it (L.C.); edoardo.proverbio@unime.it (E.P.)

\* Correspondence: parinaz.salehi@gmail.com; Tel.: +98-31-3391-5724

**Abstract:** Hard nanocrystalline Ni-Co or Ni-W coatings are receiving a growing interest owing to their premium hardness, wear, and corrosion properties for several industrial applications. Furthermore, surface hydrophobicity greatly improves surface corrosion resistance. In this research, the durability of hydrophobic hierarchical NiW electrodeposited film has been evaluated in a high-speed slurry erosion–corrosion (EC) test rig. Two different coatings have been tested: a rough coating obtained in a chloride-based bath (NiW<sub>chloride</sub>) and a smooth coating obtained in a sulfate-based bath (NiW<sub>sulfate</sub>). Corrosion behavior over time was evaluated by electrochemical impedance spectroscopy (EIS), while surface hydrophobic performance was determined by the sessile drop method. The morphological features of the coatings were assessed by scanning electron microscopy while roughness modification during the EC tests were identified by means of an atomic force microscopy. During static immersion in the aggressive solution, the impedance modulus of the coatings continuously increased due to an increase in the thickness of corrosion products. During the EC test, the impedance modulus of the smooth NiW coating decreased, losing its barrier property. It was observed that the increase in impedance modulus of the hierarchical structure of the rough NiW coating during EC was far greater than that during static immersion. After 64 min of EC, the NiW<sub>chloride</sub> was able to resume its hydrophobicity property by storing in air; nevertheless, the NiW<sub>sulfate</sub>, with a loss of approximately 72% in its initial contact angle, was no longer hydrophobic. The results showed improvements in the lifetime of hydrophobic NiW coatings in erosion–corrosion conditions of the hierarchical nanostructure obtained in a chloride-based electroplating bath.

**Keywords:** hydrophobic coating; corrosion resistance; durability; microstructural characterization; electrochemical impedance spectroscopy; contact angle



**Citation:** Salehikahrizangi, P.; Raeissi, K.; Karimzadeh, F.; Calabrese, L.; Proverbio, E. Effects of Surface Morphology on Erosion–Corrosion and Corrosion Resistance of Highly Hydrophobic Nickel-Tungsten Electrodeposited Film. *Coatings* **2021**, *11*, 1084. <https://doi.org/10.3390/coatings11091084>

Academic Editor:  
Ioannis Karapanagiotis

Received: 1 August 2021

Accepted: 31 August 2021

Published: 7 September 2021

**Publisher's Note:** MDPI stays neutral with regard to jurisdictional claims in published maps and institutional affiliations.



**Copyright:** © 2021 by the authors. Licensee MDPI, Basel, Switzerland. This article is an open access article distributed under the terms and conditions of the Creative Commons Attribution (CC BY) license (<https://creativecommons.org/licenses/by/4.0/>).

## 1. Introduction

In recent years, nanocrystalline nickel alloy coatings (e.g., Ni-W, Ni-Co) have received growing interest as an efficient replacement for hard chromium coatings for their superior hardness, wear, and corrosion properties for several applications, from microelectronics to mechanics [1,2]. Recently, an increasing number of research activities have focused on the corrosion resistance improvement of these coatings by promoting surface hydrophobicity to gain better performance in critical environmental conditions such as marine environments [3,4]. The driving force of this concept is to obtain water repellent metal surfaces and modify the anti-corrosion surface capabilities of metals and alloys, slowing down the breakage of the metal oxide film and thus preserving the metal substrate from undesired localized corrosion attack [5]. In such a context, research advances in bio-inspired non-wetting surfaces have been recently developed, focusing attention on water repellent

surfaces with a specific hierarchical (multi-scale) rough structure [6–9]. The corrosion resistance mechanism functions as follows: when exposed to an aggressive environment, the hydrophobic coatings, characterized by rough and regular hierarchical structures, can easily trap a significant amount of air within the valleys and cavities of the hierarchical surface profile [10,11]. These air pockets represent a barrier to the diffusion of aggressive ions, such as  $\text{Cl}^-$ , to the underlying metal [12–14]. The idea is appealing if corrosion is the main cause of failure in the service life of marine components. However, even with effective corrosion protection, the marine components may still suffer due to relatively low erosion resistance [15]. Therefore, the development of hydrophobic coatings with improved erosion–corrosion resistance is a matter of interest, since the low durability and stability of the hierarchical structured surfaces to the EC condition is a relevant issue that limits their practical usability in the industrial field [16–19].

Indeed, not all hydrophobic corrosion resistant coatings are suitable candidates for marine applications [15]. The low-cost polymer based hydrophobic coatings with considerable corrosion resistance are not favorable due to their weak erosion resistance and coating-to-substrate binding strength against impingement of the seawater streams. Hydrophobic metallic/ceramic coatings could be a solution to this problem [15,19–21]. The development of electroplated metal coatings with novel hydrophobic hierarchical structures and promising corrosion–wear resistance was suggested as an effective approach [19]. In this regard, hydrophobic nickel-based coatings as anti-corrosion/anti-wear protective films, thermal stable films, and electrocatalysts are of practical importance in industrial sectors [1,22]. However, despite the promising results about the effect of hydrophobicity on improving the corrosion resistance of nickel-based coatings [23–26], the overall contribution of hydrophobicity to erosion–corrosion durability and the stability of nickel-based coatings is still under debate. During the early stages of exposure to the erosion–corrosion (EC) condition, the hierarchical structure of nickel coating could be seriously degraded with a consequent loss of the hydrophobic properties [19]. The improvement in the stability of surface nanostructure is therefore of primary importance.

The aim of the present work is to evaluate how tungsten alloying in electrodeposited Ni coating could improve surface morphology stability. Since it is well known that the composition of the bath could significantly influence the coating nanostructure [27], two different bath solutions were adopted for electrodeposition [28]. Using morphological and electrochemical investigations, the influence of the microstructure of NiW electrodeposited film on the EC test durability was assessed. In particular, in situ real time electrochemical measurements have been performed during the EC test. The results were compared with corrosion behavior in stationary solution to discriminate the contribution of erosion and corrosion to degradation phenomena.

## 2. Materials and Methods

NiW coatings were deposited on copper discs (exposed area:  $3.14 \text{ cm}^2$ ) in two different chloride-based ( $\text{NiW}_{\text{chloride}}$ ) and sulfate-based ( $\text{NiW}_{\text{sulfate}}$ ) baths whose compositions are detailed in [28]. The electrodeposition process was galvanostatically conducted at  $60 \text{ }^\circ\text{C}$  under a rotation speed of 300 rpm using a potentiostat–galvanostat (AMEL 2053 by Amel Electrochemistry, Milano, Italy) [28].

Morphological features on the surface of all electroplated batches were assessed using a dual-beam scanning microscope (FIB-SEM Crossbeam 540, ZEISS, Italy). For all batches, the changes in roughness during the EC tests were acquired by means of an atomic force microscope (AFM, VEECO Explorer, Veeco Instruments, Munich, Germany) using a nonconductive silicon nitride probe (MSCT-EXMT-BF1, Veeco Instruments, Munich, Germany), operating in contact mode.

A tensiometer (Attension Theta, Biolin Scientific, Stockholm, Sweden) was employed to study the surface hydrophobic performances of the sample surfaces by the sessile drop method. A water droplet (volume  $2 \text{ } \mu\text{L}$ ) was placed on the surface open to the air ( $25 \text{ }^\circ\text{C}$ ). Deposition images of the droplet, recorded by a micro-camera device, were further

elaborated with a suitable digital image software (PC Attension Theta software, Rev. 1.7, 2012 by Biolin Scientific, Stockholm, Sweden) to acquire the static water contact angle. For each batch, five replicas were performed.

Electrochemical measurements were carried out in a 3.5 wt% NaCl solution using a BioLogic SP-300 potentiostat (BioLogic, Paris, France) and a three-electrode cell configuration (where the coated sample is the working electrode; a KCl-saturated Ag/AgCl reference electrode probe was utilized; an activated titanium mesh was employed as a counter electrode). The potentiodynamic polarization curves were plotted in the range  $-50$  to  $\pm 1500$  mV from open circuit potential (OCP) with a scan rate of 1 mV/s. Impedance measurements were conducted using a voltage amplitude equal to 10 mV vs. OCP and a frequency range of  $10^5$ – $10^{-1}$  Hz.

Erosion–corrosion (EC) tests were performed using the test rig represented in Figure 1. The setup consists of a glass beaker including 1 L solution. In particular, the solution slurry was obtained by mixing 3.5 wt% NaCl with 40 wt% glass grinding filler (average diameter 200–300  $\mu\text{m}$ ). A DC rotary motor is connected to a plastic blender, which throws the sand particles with a constant rotational speed (500 rpm) at the sample surface. Details about the erosion–corrosion set up and the sample/electrodes schematic position are reported in reference [19].

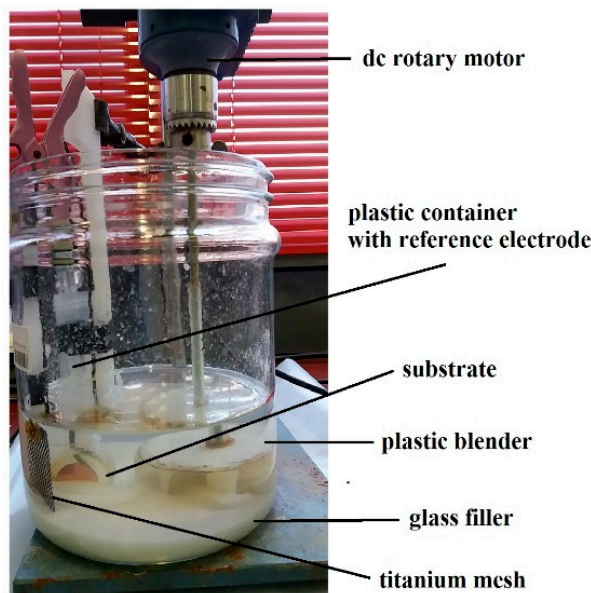


**Figure 1.** Test rig used for erosion–corrosion experiments.

On-site electrochemical impedance spectroscopy (EIS) was performed using a three-electrode configuration (coated sample as working electrode; Ag/AgCl probe as reference electrode; activated titanium mesh as a counter electrode). More details about the EC tests and the test set up can be found in reference [19]. With the purpose to determine the water contact angle (WCA) of the samples after each cycle of erosion–corrosion, they were removed from slurry solution, washed with deionized water, dried, and rested for two weeks in open to air conditions.

### 3. Results and Discussion

#### 3.1. Morphology and Surface Considerations by SEM

Different electrodeposition bath compositions resulted in different morphological features, as can be observed in SEM images in Figure 2.  $\text{NiW}_{\text{chloride}}$  is characterized by a fully rough surface structure consisting of micro popcorns covered by nano flakes homogeneously spread all over the surface (Figure 2a). On the contrary,  $\text{NiW}_{\text{sulfate}}$  consists of many smooth islands with occasional cracks between two interconnecting islands.

The details about the microstructural characterization of NiW coatings are reported in reference [28].

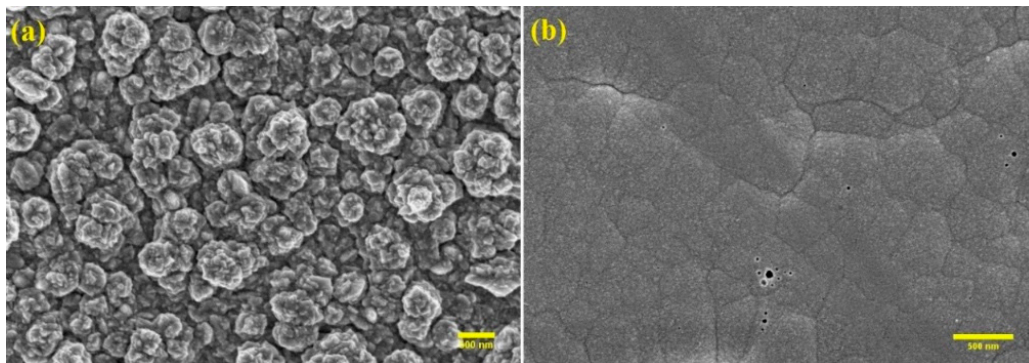


**Figure 2.** SEM images of surface morphologies of electrodeposited (a) NiW<sub>chloride</sub> and (b) NiW<sub>sulfate</sub> coatings.

### 3.2. Corrosion Resistance of the Coatings

#### 3.2.1. Polarization Readings

The effect of tungsten alloying element on the stability of nickel coatings, electrodeposited from both sulfate and chloride baths, at varying electrochemical potentials was investigated through DC polarization tests (Figure 3). For NiW<sub>chloride</sub> and NiW<sub>sulfate</sub> coatings, the corrosion potential ( $E_{\text{corr}}$ ) values are  $-285.8$  and  $-227.5$  mV<sub>Ag/AgCl</sub>, respectively. The less noble corrosion potential is observed for NiW<sub>chloride</sub> coating. Considering that, in PDM, the logarithm of the steady-state current generally varies linearly with the applied voltage (Tafel relation), the aforementioned variation in trend of current within the anodic branch should be due to the change in the oxidation state of cations within the films [29,30]. However, the formation of insoluble corrosion products could lead to the formation of a protective layer able to separate the aggressive electrolyte from the metallic NiW coating or substrate and prevent the corrosion of NiW coating [31]. The oxide film is constituted mainly by Ni(OH)<sub>2</sub>, NiO, and WO<sub>3</sub> oxide/hydroxide by Raman analyses [32].

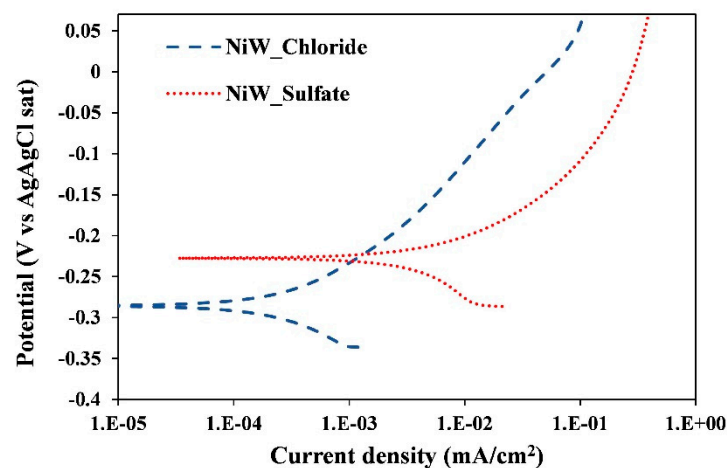


**Figure 3.** Potentiodynamic polarization curves of NiW coatings in neutral 3.5 wt% NaCl solution (areas on X-axis are visible and not real).

Table 1 compares the apparent corrosion current density ( $i_{\text{corr}}$ ) and  $E_{\text{corr}}$  values of the coatings obtained using the linear polarization method. Based on the results of Table 1, NiW<sub>chloride</sub>, with lower apparent corrosion current density ( $i_{\text{corr}}$ ) or higher polarization resistance ( $R_p$ ) [19], is more corrosion resistant than NiW<sub>sulfate</sub>. Since W contents of both coatings are quite similar ( $\leq 10$  at%) [28], the reason for this difference in corrosion resistance must be related to the surface structure. Farzaneh et al. [33] also related the variations in

$i_p$  of NiW coatings to the changes in surface structure rather than the effect of alloying with W. Therefore, the improved corrosion resistance of NiW<sub>chloride</sub> coating, compared to that of NiW<sub>sulfate</sub> coating, can be related to its new popcorn morphology [28]. It should be remarked that the morphology affects the surface characteristics of the electroplated films, which influences the exchange current density of half-cell reactions in the corrosion process.

**Table 1.** Corrosion parameters for NiW coatings (areas are visible and not real).

Parameter	Chloride	Sulfate
$E_{\text{corr}}$ (mV)	−285.8	−227.5
$R_p$ (ohm/cm <sup>2</sup> )	77.091	5774
$i_{\text{corr}}$ (mA/cm <sup>2</sup> )	$3.4 \times 10^{-4}$	$4.5 \times 10^{-3}$

### 3.2.2. EIS Studies of the Coatings

EIS plots of the electrodeposited coatings during 64 min of static corrosion were studied (Figure 4) to better assess the effect of immersion time on electrochemical behavior of the films. The increase in loop diameter in Nyquist plots of both coatings during static immersion in aggressive solution is due to improvements in barrier action (Figure 4a,c). Additionally, a pseudo-passive oxide layer due to corrosion products could be responsible for the appearance of the wide humps in bode-phase plots (Figure 4b,d). In fact, the humps represent the capacitive responses of this protective oxide layer, which shift to the higher angles by increasing the immersion time due to their thickening (Figure 4b,d). This proves the emerging effect of a pseudo-passivity on corrosion performance of the electrodeposited film during the immersion.

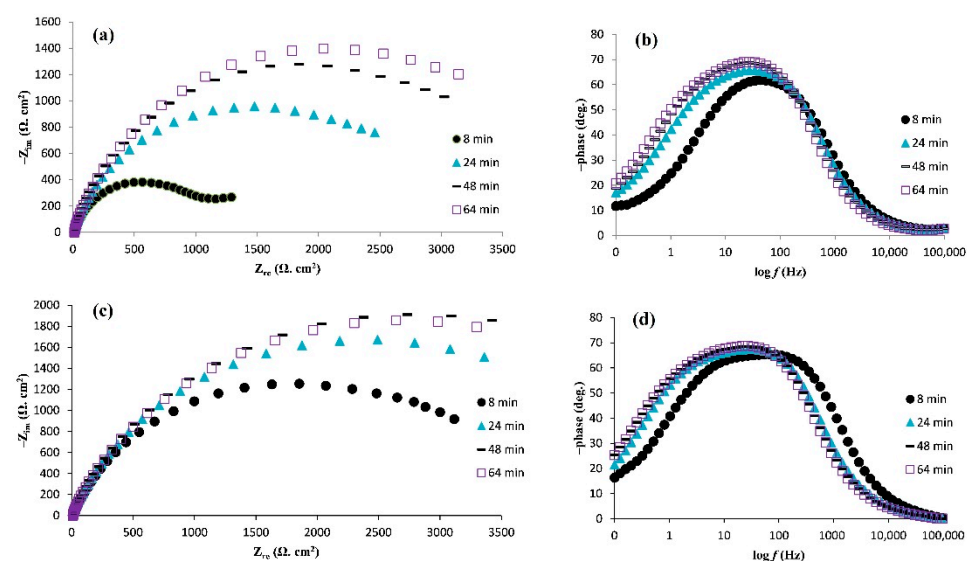


**Figure 4.** Nyquist and Bode plots of (a,b) NiW<sub>chloride</sub> and (c,d) NiW<sub>sulfate</sub> coatings during 64 min of corrosion.

### 3.3. Erosion–Corrosion Behavior of the Electrodeposited Coatings

#### 3.3.1. OCP vs. Time

The OCP of the coatings at increasing time during EC tests is reported in Figure 5. Different trends observed for the two coatings could be due to differences in their real and local surface compositions (number of grains/boundaries and the relative fraction of different elements at the surface). Moreover, OCP changes over each coating system are typically related to the permeation of water, oxygen, and ions. Therefore, the OCP vs. exposure time direction cannot be easily predicted. The continuous modification of the surface morphology and the turbulence at the surface could significantly influence OCP measurements that we can consider in a nonstationary condition. It is noticeable

to observe that the NiW<sub>chloride</sub> coating is characterized by a gradual depolarization of the surface, while the NiW<sub>sulfate</sub> coating shows an increase in OCP values. Both values gradually converge toward an asymptotic similar value. The results are reflected also in the different behavior of the coating under EIS characterization.

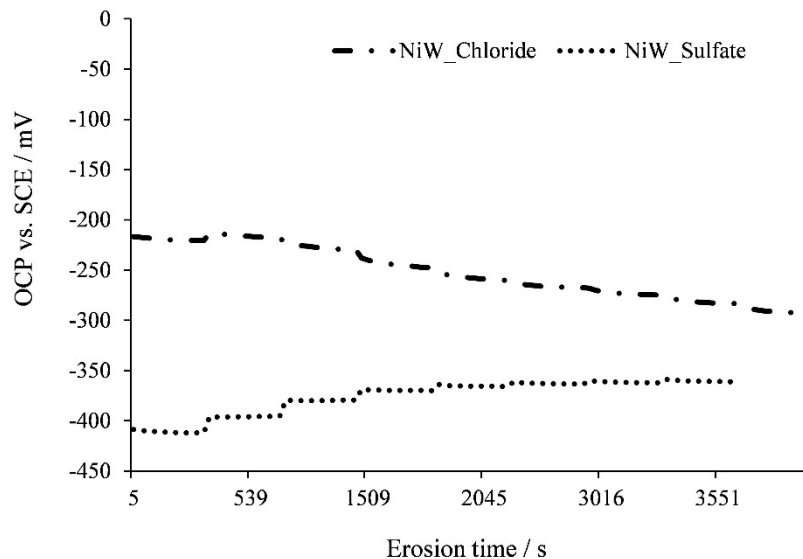


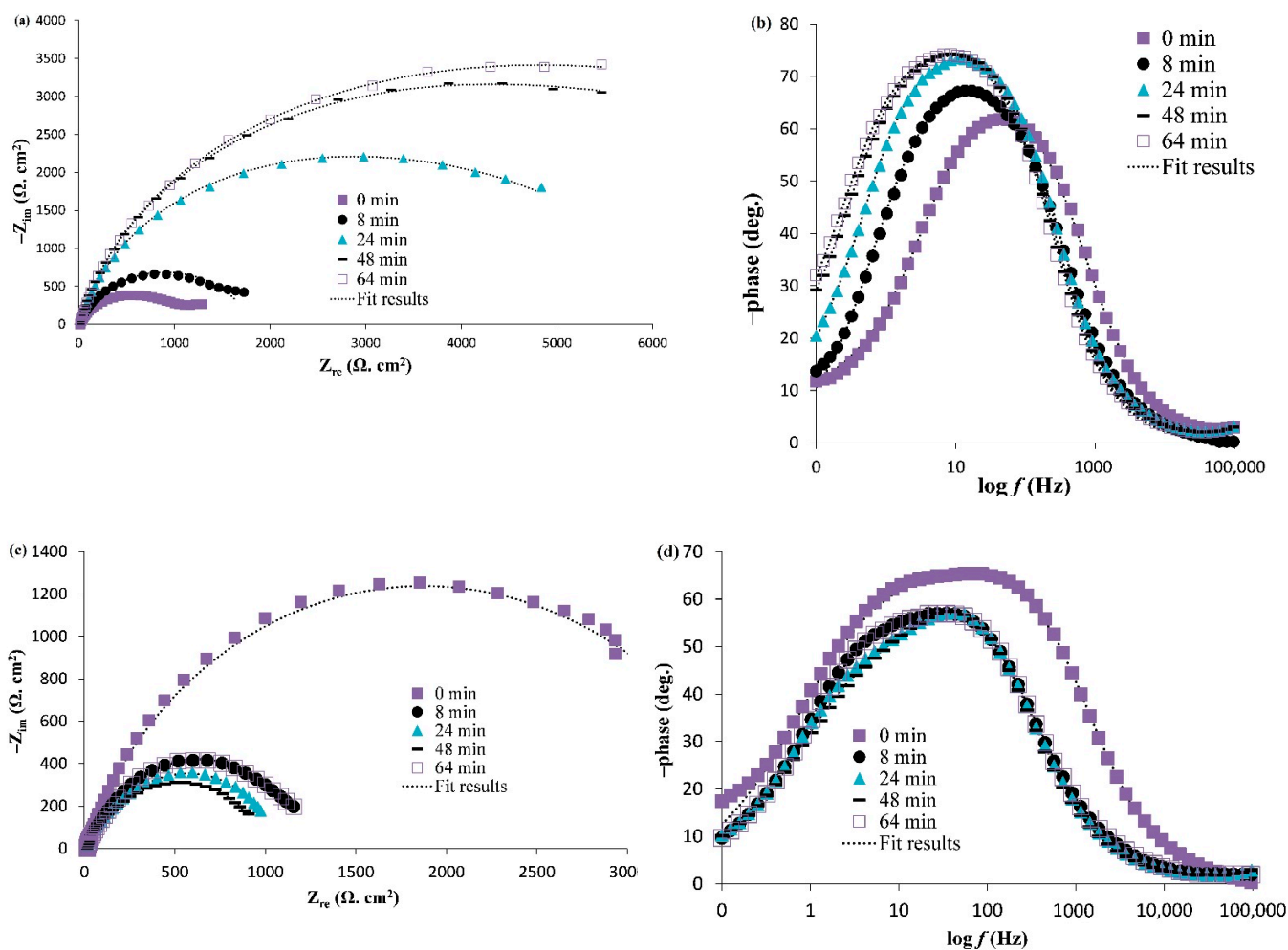
**Figure 5.** Changes in the OCPs of the coated samples during erosion–corrosion test.

### 3.3.2. EIS Characterization

Figure 6 shows the EIS plots of the NiW<sub>chloride</sub> and NiW<sub>sulfate</sub> coatings before EC (0 min, in static slurry solution) and during EC aging up to 64 min. The loop diameter in the Nyquist plot of the NiW<sub>chloride</sub> coating at various EC times (Figure 6a) is much larger than that obtained in similar periods in the static corrosion test (Figure 4a). Taking into account that the same solution is used for both tests, the higher impedance modulus obtained during the EC must be directly related to the changes that occurred in roughness under impingement of the glass grinding filler particles.

A progressive increase in the impedance magnitude of the NiW<sub>chloride</sub> by increasing erosion time is observed (Figure 6a), while it considerably decreases with the start of erosion in the case of the NiW<sub>sulfate</sub> (Figure 6c) unlike its behavior during the static corrosion test (Figure 4c). By comparing the impedance trends of the films at long EC time (64 min), it is noted that the impedance modulus of the NiW<sub>chloride</sub> coating (Figure 6a) is significantly higher than that of the NiW<sub>sulfate</sub> (Figure 6c). This means that the healing (by oxide growth) ability of the NiW<sub>chloride</sub> after erosion damages resulted in erosion cycles higher than the NiW<sub>sulfate</sub>. In Bode-phase plots (Figure 6b,d), the near wide peaks at approximately 10 Hz for the NiW<sub>chloride</sub> coating and approximately 100 Hz for the NiW<sub>sulfate</sub> coating correspond to a time constant, which represents the electrochemical response of the protective film. At the beginning of the erosion–corrosion test, the maximum phase angle of the NiW<sub>chloride</sub> coating (Figure 6b) is approximately 60°, which reaches approximately 75° after 24 min of erosion and remains almost constant up to long EC time. This increase in the phase angle of the NiW<sub>chloride</sub> coating indicates that the capacitive response of the coating is exalted, enhancing its pseudo-passivity [33]. For the NiW<sub>sulfate</sub> coating (Figure 6d), a continuous decrease in maximum phase angle from approximately 65° in the beginning of the EC test to approximately 55° after 8 min of erosion is obvious. This denotes the decay of barrier properties of this coating. After 8 min, and until 64 min (the maximum chosen EC time), the phase angle remains constant. The different impedance behavior of the electrodeposited films during the erosion–corrosion test can be ascribed to the different attitude of the NiW coating in NaCl solution. Tungsten forms many relatively insoluble complexes with chloride ions, and its protecting factor is a result of its probable reaction with chloride, which fills the pores with a film of corrosion products. Tungsten

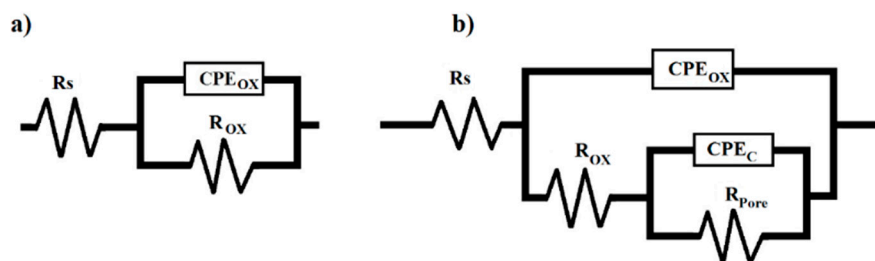
has domains of passivity associated with  $\text{WO}_2$  and  $\text{WO}_3$  with the latter material having low solubility and being stable to further oxidation [34]. These protective films, constituted mainly by metal oxide/hydroxides, separate the coating surface from electrolyte and raise the impedance modulus of the coating during immersion time [31]. The reduction in impedance modulus during the erosion of the  $\text{NiW}_{\text{sulfate}}$  coating can be related to the less stable protective layer triggered for this coating because of the presence of large cracks and defects on its surface. The presence of surface cracks is responsible for the local metal dissolution.



**Figure 6.** Nyquist and Bode plots of (a,b)  $\text{NiW}_{\text{chloride}}$  and (c,d)  $\text{NiW}_{\text{sulfate}}$  coatings before erosion–corrosion (0 min) and during 64 min of erosion–corrosion tests.

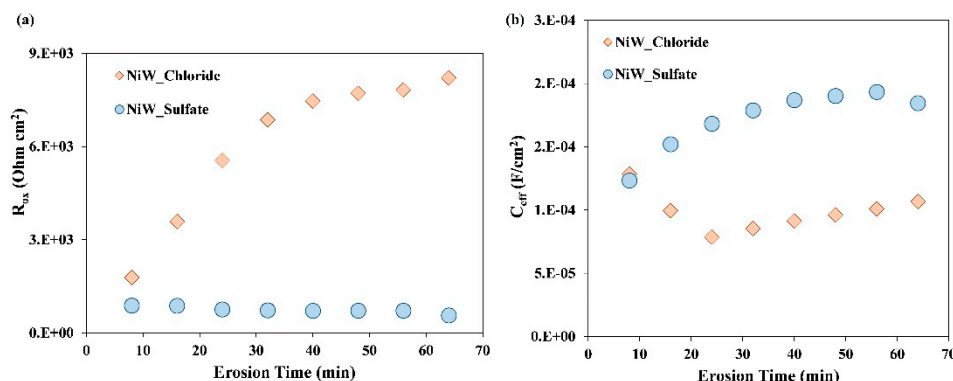
### 3.3.3. EIS Modeling

Figure 7 represents the equivalent circuits corresponding to EIS plots of the  $\text{NiW}$  coatings.  $R_s$  is the uncompensated resistance of the electrolyte,  $R_{\text{ox}}$  and  $\text{CPE}_{\text{ox}}$  are the resistance and the constant phase element (CPE) of the protective oxide layer, respectively. The capacitors are usually replaced by the CPE to represent deviations from ideal capacitive behavior. In Figure 7b,  $R_{\text{pore}}$  and  $\text{CPE}_c$  represent the pore resistance and the CPE relating to pores and cracks in the  $\text{NiW}_{\text{sulfate}}$  coating. As shown in Figure 6, a suitable correlation between experimental (solid markers points) and fitted results (solid lines) was attained using the proposed electrical equivalent circuits.



**Figure 7.** Scheme of the electrical equivalent circuits corresponding to EIS plots of: (a) NiW<sub>chloride</sub> and (b) NiW<sub>sulfate</sub> coatings.

Figure 8a compares the simulated  $R_{ox}$  values of the NiW coatings extracted from Figure 6 using the equivalent circuits (Figure 7). As seen in Figure 8a and after 30 min of EC,  $R_{ox}$  values for the NiW<sub>chloride</sub> coating are approximately nine times higher than those obtained for the NiW<sub>sulfate</sub> coating. Therefore, the hierarchically rough NiW<sub>chloride</sub> coating provides stronger protection during erosion–corrosion tests than the smooth NiW<sub>sulfate</sub> one. The  $R_{ox}$  of the films could also be inversely related to the real exposed surface area (ESA) of the coating. Therefore, the sharp increase in  $R_{ox}$  of the NiW<sub>chloride</sub> coating at the start of the erosion–corrosion test (Figure 8a) may also be related to the sudden decrease in ESA of this coating, related to the progressive loss of the hierarchical structured profile of the electrodeposited surface. In this case, and during the early stages of erosion–corrosion, the electrolyte penetrates inside the valleys and cavities of the rough NiW<sub>chloride</sub> coating surface. By increasing erosion time, due to the gradual loss of the surface asperities, the ESA of the coating decreases sufficiently, and a smoother surface is obtained. This may explain the intensive increase in  $R_{ox}$  of the NiW<sub>chloride</sub> vs. erosion time (Figure 8a). This increase is considerable after the first cycle (8 min), where the highest loss of roughness (~38%) was reached. Further details about roughness changes in the electrodeposited films during erosion–corrosion will be discussed in Section 3.4. Because all coatings change to hydrophilic (or the hydrophobic behavior is less effective) after approximately 8 min of immersion in the aggressive solution, as mentioned in Figure 3, the authors do not relate the superior corrosion resistance of NiW<sub>chloride</sub> coating to the hydrophobicity character of the coatings. Moreover, during this short period of the hydrophobicity, the impedance of the coatings is still not very high. Therefore, the changes in the  $R_{ox}$  value of the coatings should be caused by changes in the film surface (i.e., reduction in roughness) during the EC test.



**Figure 8.** Changes in: (a)  $R_{ox}$  and (b)  $C_{eff}$  values for NiW<sub>chloride</sub> and NiW<sub>sulfate</sub> coatings during EC.

In order to easily compare the protective action of the two coatings, the effective capacitance ( $C_{eff}$ ) was calculated [35,36] and reported in Figure 8b.  $C_{eff}$  can be obtained from the following expression:

$$C_{eff} = CPE_{ox}^{\frac{1}{\alpha}} \times R_{Pore}^{\frac{(1-\alpha)}{\alpha}} \tag{1}$$

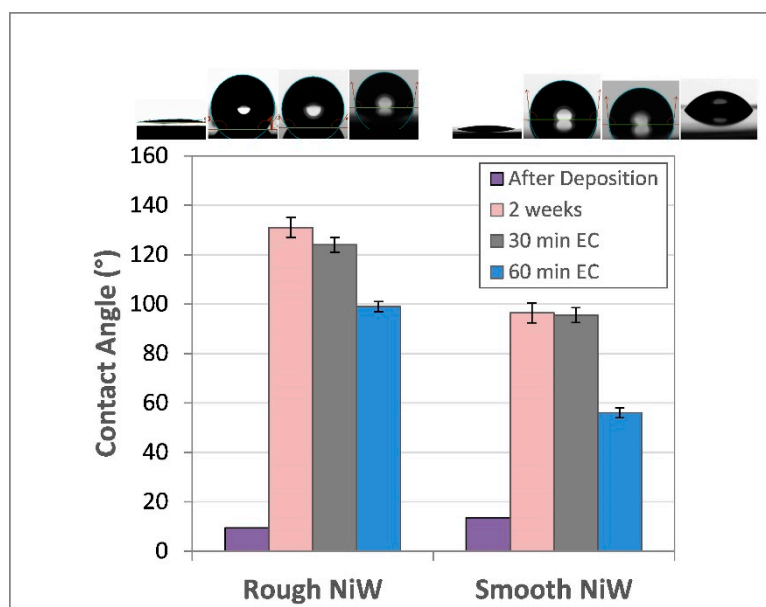
where  $\alpha$  is the  $CPE_{ox}$  power and has a value between 0 (pure resistance) and 1 (pure capacitance).

A wide difference in the capacitive behavior of the two NiW coatings can be observed in Figure 8. According to this Figure, the  $C_{eff}$  values of the NiW<sub>chloride</sub> are much lower than those obtained for the NiW<sub>sulfate</sub> coating, indicating its higher barrier performance. The NiW<sub>chloride</sub> coating is characterized by a hierarchical morphology with an effective barrier action [28]. Although there are erosion effects on the specimen even after short times, the electrochemical behavior of the coating is still satisfactory, owing to its high self-healing behavior after the sand mechanical action that modifies the surface roughness [37]. For the NiW<sub>chloride</sub> coating, although there is a progressive loss of its hierarchical structure morphology, it still exhibits a good electrochemical stability. On the other hand, despite showing a low roughness variation during erosion, the NiW<sub>sulfate</sub> has intrinsic defects [28] that undermine its barrier capacity. Thus, this makes it possible to retain the hydrophobic NiW<sub>chloride</sub> coatings that are potentially effective for their use even in heavy industrial fields.

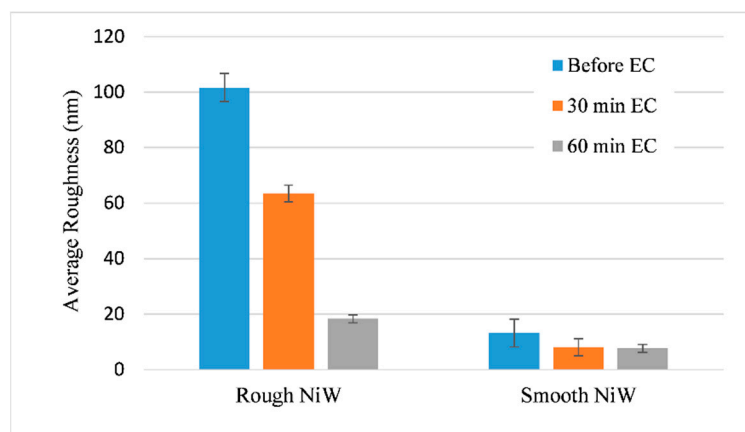
### 3.4. Hydrophobicity and Roughness of the Coatings

Figure 9 shows the WCA changes in the NiW electrodeposited films at varying ageing steps: (i) quickly after electrodeposition; (ii) after two storage weeks in air; (iii) after 30 min of erosion–corrosion (EC) test; and (iv) after 60 min of erosion–corrosion (EC) test. As can be observed, both NiW coatings are hydrophilic just after electroplating and become hydrophobic after two weeks' storage in air. The transition from hydrophilic to hydrophobic behavior, although there are still some controversies about it [38], could occur due to the spontaneous adsorption of organic molecules (airborne organic hydrocarbons) on high surface energy areas [39]. The adsorption of nonpolar airborne hydrocarbons decreases the surface energy of the electrodeposited metal coating, increasing its hydrophobic behavior with subsequent increase in the WCA [40]. After two storage weeks open to air, the WCA of the rough NiW<sub>chloride</sub> coating ( $130^\circ$ ) was approximately  $35^\circ$  higher than that of the smooth NiW<sub>sulfate</sub> ( $95^\circ$ ). This behavior can be ascribed to the hierarchical nature of the NiW<sub>chloride</sub> coating compared to the NiW<sub>sulfate</sub> one. In a rough surface, based on the Cassie–Baxter theory, the air pockets trapped in the surface asperities may take place, thereby reducing the actual contact surface of the water droplet and resulting in a higher WCA [41]. Evaluating the wettability properties of NiW<sub>chloride</sub> coating after 30 min of EC (after removing, washing, drying, and two weeks of storage) showed a decrease of approximately  $7^\circ$  (~5% lost) in its contact angle due to the partial erosion of its hierarchical structure. In the case of NiW<sub>sulfate</sub>, only a decrease of approximately  $1^\circ$  (~1% lost) in its contact angle is observed. After 64 min of EC, NiW<sub>chloride</sub> can resume its hydrophobicity property by storing in air; nevertheless, NiW<sub>sulfate</sub>, with a loss of approximately 72% in its initial contact angle, will not be hydrophobic anymore. The loss of contact angle and transition to the fully hydrophilic region during EC tests was already detected for nickel coatings with hierarchical/smooth structures in the same testing condition [19].

Changes in WCA of NiW electrodeposited films (Figure 9) are in accordance with the variations in their average roughness (Figure 10), resulting from the EC test. approximately 38% of the early average roughness of the NiW coating is lost just after 30 min of EC (Figure 10). In similar research and the absence of tungsten alloying element, nickel lost approximately 65% of its initial hierarchical roughness [19]. Therefore, tungsten seems successful in better surviving the hierarchical rough structure of nickel against erosion damage. After 64 min of EC, approximately 82% of the initial roughness of the NiW<sub>chloride</sub> coating is lost (Figure 10). At this time, the coating can still resume hydrophobicity by storing in the air (Figure 9). In the case of the smooth NiW<sub>sulfate</sub> coating, changes in its roughness are trivial, but the coating turns hydrophilic after 64 min of EC, as similarly observed for smooth Ni coating [19].



**Figure 9.** Changes in the water contact angle of NiW coatings quickly after electrodeposition, after two storage weeks in air and after erosion–corrosion (after removing, washing, drying and two weeks of storage in the air).



**Figure 10.** The average roughness of the NiW coatings before and after EC tests, as evidenced by AFM observation.

Figure 11 explains how tungsten affects the loss both in roughness and hydrophobicity in nickel coating with increasing erosion time. By adding tungsten, despite the lower initial roughness of the NiW<sub>chloride</sub> coating, the slope is moderate, and the coating resumes its hydrophobicity after each erosion step by a storing cycle in air.

By studying roughness results of Ni [19] and NiW coatings, both obtained by electrodeposition in chloride baths, it is observed that Ni coating is characterized by an initial average roughness of higher than 250 nm. However, the initial roughness of NiW coating is ~100 nm, which is ~150% lower than Ni one. Furthermore, by increasing the erosion time, Ni coating shows an abrupt reduction in its average roughness. The gap highlighted between roughness values of two coatings before erosion (0 min) is practically filled just after 30 min of erosion. After 30 min of erosion, Ni coating has a roughness reduction of ~150%, unlike NiW, where a reduction of only 65% occurred. This trend was, afterward, confirmed at 64 min of erosion. Finally, NiW coating displays a higher contact angle than Ni coating after the end of the test.

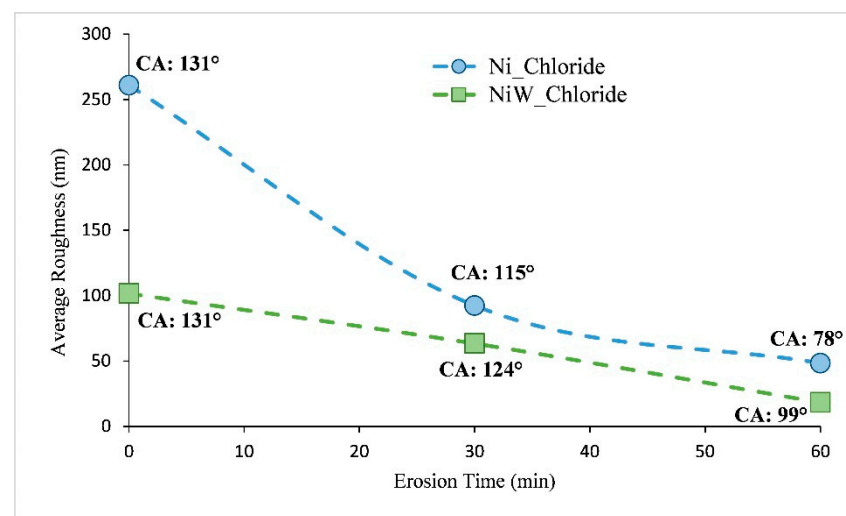


**Figure 11.** Effect of tungsten on changes in the average roughness of Ni [19] and NiW coatings.

#### 4. Conclusions

In this paper, the effect of tungsten on the durability of hydrophobic hierarchical structure of nickel during high-speed EC tests was studied. For this purpose, chloride- and sulfate-based baths were used to develop rough and smooth NiW coatings, respectively. The corrosion and erosion–corrosion behaviors of coatings were studied, and the following results were obtained:

- During static immersion in aggressive solution, due to the thickening of the corrosion products, barrier properties of both coatings increased, regardless of their different morphologies. During EC, the smooth NiW coating lost its barrier property whereas the barrier action of the rough NiW coating exceeded its value during static immersion.
- The hierarchical structure obtained from the chloride-based electrolyte improved durability of hydrophobicity behavior of NiW coatings during EC tests. In this regard, the NiW<sub>chloride</sub> resumed its hydrophobicity by storing in the air after EC tests. However, the NiW<sub>sulfate</sub> lost approximately 72% of its initial contact angle after EC and was not hydrophobic anymore.
- The capacitive behavior of the two NiW coatings was widely different. The  $C_{eff}$  values of the NiW<sub>chloride</sub> were much lower than those obtained for the NiW<sub>sulfate</sub> coating each time, indicating the higher barrier performance of hierarchical morphology.

**Author Contributions:** K.R. conceptualized the main idea; P.S., K.R., L.C. and E.P. designed and performed the methodology; K.R., E.P. and F.K. provided the resources; P.S. investigated the results; P.S., K.R., F.K., L.C. and E.P. validated the experimental data; L.C. and P.S. performed the software analysis; K.R., L.C. and E.P. performed the formal analysis; P.S. and L.C. performed the data curation; P.S. wrote and prepared the original draft; K.R., F.K., L.C. and E.P. reviewed and edited the draft; K.R. and E.P. supervised the whole work. All authors have read and agreed to the published version of the manuscript.

**Funding:** This research received no external funding. The APC was funded by University of Messina, Messina, Italy.

**Institutional Review Board Statement:** Not applicable.

**Informed Consent Statement:** Not applicable.

**Data Availability Statement:** All experimental data are stored at Department of Materials Engineering of Isfahan University of Technology.

**Conflicts of Interest:** The authors declare no conflict of interest.

## Nomenclature

EC	erosion–corrosion
OCP	open circuit potential
EIS	electrochemical impedance spectroscopy
WCA	water contact angle
DC polarization	direct current polarization
$E_{corr}$	corrosion potential
$i_{corr}$	apparent corrosion current density
$R_p$	polarization resistance
$CPE_{ox}$	constant phase element of the passive oxide
$CPE_c$	constant phase element of cracks and pores in coating
$R_s$	electrolyte resistance
$R_{ox}$	passive oxide resistance
$R_{pore}$	pore resistance
ESA	exposed surface area
$C_{eff}$	effective capacitance
$\alpha$	constant phase element power

## References

- Allahyarzadeh, M.H.; Aliofkhaezrai, M.; Rezvanian, A.R.; Torabinejad, V.; Rouhaghdam, A.R.S. Ni-W electrodeposited coatings: Characterization, properties and applications. *Surf. Coat. Tech.* **2016**, *307*, 978–1010. [[CrossRef](#)]
- Karimzadeh, A.; Aliofkhaezrai, M.; Walsh, F.C. A review of electrodeposited Ni-Co alloy and composite coatings: Microstructure, properties and applications. *Surf. Coat. Tech.* **2019**, *372*, 463–498. [[CrossRef](#)]
- Liu, T.; Yin, Y.S.; Dong, L.H. New application of the “underwater super-hydrophobic” surface in the corrosion protection. *Adv. Mater. Res.* **2009**, *79–82*, 1115–1118. [[CrossRef](#)]
- Ferrari, M.; Benedetti, A. Superhydrophobic surfaces for applications in seawater. *Adv. Colloid Interface Sci.* **2015**, *222*, 291–304. [[CrossRef](#)] [[PubMed](#)]
- Mohamed, A.M.A.; Abdullah, A.M.; Younan, N.A. Corrosion behavior of superhydrophobic surfaces: A review. *Arab. J. Chem.* **2015**, *8*, 749–765. [[CrossRef](#)]
- Khorsand, S.; Raeissi, K.; Ashrafzadeh, F.; Arenas, M.A. Relationship between the Structure and Water Repellency of Nickel–Cobalt Alloy Coatings Prepared by Electrodeposition Process. *Surf. Coat. Technol.* **2015**, *276*, 296–304. [[CrossRef](#)]
- Hashemzadeh, M.; Raeissi, K.; Ashrafzadeh, F.; Khorsand, S. Effect of ammonium chloride on microstructure, super-hydrophobicity and corrosion resistance of nickel coatings. *Surf. Coat. Tech.* **2015**, *283*, 318–328. [[CrossRef](#)]
- Nosonovsky, M.; Bhushan, B. Hierarchical roughness optimization for biomimetic superhydrophobic surfaces. *Ultramicroscopy* **2007**, *107*, 969–979. [[CrossRef](#)]
- Hang, T.; Hu, A.; Ling, H.; Li, M.; Mao, D. Super-hydrophobic nickel films with micro-nano hierarchical structure prepared by electrodeposition. *Appl. Surf. Sci.* **2010**, *256*, 2400–2404. [[CrossRef](#)]
- Xu, X.H.; Zhang, Z.Z.; Yang, J.; Zhu, X.T. Study of the corrosion resistance and loading capacity of superhydrophobic meshes fabricated by spraying method. *Colloid. Surf. A Physiochem. Eng. Asp.* **2011**, *377*, 70–75. [[CrossRef](#)]
- Vazirinasab, E.; Jafari, R.; Momen, G. Application of superhydrophobic coatings as a corrosion barrier: A review. *Surf. Coat. Tech.* **2018**, *341*, 40–56. [[CrossRef](#)]
- Toloei, A.S.; Stoilov, V.; Northwood, D.O. *The Relationship between Surface Roughness and Corrosion*; International Mechanical Engineering Congress and Exposition; ASME: New York, NY, USA, 2013; pp. 1–10.
- Herminghaus, S. Roughness-induced non-wetting. *Europhys. Lett.* **2000**, *52*, 165–170. [[CrossRef](#)]
- Quere, D. Wetting and roughness. *Annu. Rev. Mater. Res.* **2008**, *38*, 71–99. [[CrossRef](#)]
- Wang, Y.; Zheng, Y.G.; Ke, W.; Sun, W.H.; Hou, W.L.; Chang, X.C. Slurry erosion–corrosion behaviour of high-velocity oxy-fuel (HVOF) sprayed Fe-based amorphous metallic coatings for marine pump in sand-containing NaCl solutions. *Corros. Sci.* **2011**, *53*, 3177–3185. [[CrossRef](#)]
- Bayer, I.S. On the durability and wear resistance of transparent superhydrophobic coatings. *Coatings* **2017**, *7*, 12. [[CrossRef](#)]
- Garcia-Giron, A.; Romano, J.M.; Batal, A.; Dashtbozorg, B.; Dong, H.; Solanas, E.M. Durability and wear resistance of laser-textured hardened stainless steel surfaces with hydrophobic properties. *Langmuir* **2019**, *35*, 5353–5363. [[CrossRef](#)]
- Xiao, S.; Hao, X.; Yang, Y.; Li, L.; He, N.; Li, H. Feasible fabrication of a wear-resistant hydrophobic surface. *Appl. Surf. Sci.* **2019**, *463*, 923–930. [[CrossRef](#)]
- Salehikahrizsanghi, P.; Raeissi, K.; Karimzadeh, F.; Calabrese, L.; Patane, S.; Proverbio, E. Erosion-corrosion behavior of highly hydrophobic hierarchical Nickel coatings. *Colloid. Surf. A Physiochem. Eng. Asp.* **2018**, *558*, 446–454. [[CrossRef](#)]
- Calderón, J.A.; Henao, J.E.; Gómez, M.A. Erosion–corrosion resistance of Ni composite coatings with embedded SiC nanoparticles. *Electrochim. Acta* **2014**, *124*, 190–198. [[CrossRef](#)]

21. Burstein, G.T.; Sasaki, K. Effect of impact angle on the slurry erosion–corrosion of 304L stainless steel. *Wear* **2000**, *240*, 80–94. [[CrossRef](#)]
22. Kumar, U.P.; Shanmugan, S.; Kennady, C.J.; Shibli, S.M.A. Anti-corrosion and microstructural properties of Ni–W alloy coatings: Effect of 3,4-Dihydroxybenzaldehyde. *Heliyon* **2019**, *5*, e01288. [[CrossRef](#)]
23. Khorsand, S.; Raeissi, K.; Ashrafizadeh, F. Corrosion resistance and long-term durability of superhydrophobic nickel film prepared by electrodeposition process. *Appl. Surf. Sci.* **2014**, *305*, 498–505. [[CrossRef](#)]
24. She, Z.; Li, Q.; Wang, Z.; Tan, C.; Zhou, J.; Li, L. Highly anticorrosion, self-cleaning superhydrophobic Ni–Co surface fabricated on AZ91D magnesium alloy. *Surf. Coat. Technol.* **2014**, *251*, 7–14. [[CrossRef](#)]
25. Liu, T.; Yin, Y.; Chen, S.; Chang, X.; Cheng, S. Super-hydrophobic surfaces improve corrosion resistance of copper in seawater. *Electrochim. Acta* **2007**, *52*, 3709–3713. [[CrossRef](#)]
26. Esmailzadeh, S.; Khorsand, S.; Raeissi, K.; Ashrafizadeh, F. Microstructural evolution and corrosion resistance of superhydrophobic electrodeposited nickel films. *Surf. Coat. Tech.* **2015**, *283*, 337–346. [[CrossRef](#)]
27. Younes-Metzler, O.; Zhu, L.; Gileadi, E. The anomalous codeposition of tungsten in the presence of nickel. *Electrochim. Acta* **2003**, *48*, 2551–2562. [[CrossRef](#)]
28. Salehikahrizsangi, P.; Raeissi, K.; Karimzadeh, F.; Calabrese, L.; Proverbio, E. Highly hydrophobic Ni–W electrodeposited film with hierarchical structure. *Surf. Coat. Tech.* **2018**, *344*, 626–635. [[CrossRef](#)]
29. Macdonald, D.D. The point defect model for the passive state. *J. Electrochem. Soc.* **1992**, *139*, 3434–3449. [[CrossRef](#)]
30. Sikora, E.; Macdonald, D.D. Nature of the passive film on nickel. *Electrochim. Acta* **2002**, *48*, 69–77. [[CrossRef](#)]
31. Wang, M. Electrodeposited free-crack NiW films under super gravity filed: Structure and excellent corrosion property. *Mater. Chem. Phys.* **2014**, *148*, 245–252. [[CrossRef](#)]
32. Correia, A.; Barros, E.; Colares, R. Morphological, structural, microhardness and electrochemical characterisations of electrodeposited Cr and Ni–W coatings. *Electrochim. Acta* **2010**, *55*, 2078–2086.
33. Calabrese, L.; Bonaccorsi, L.; Capri, A.; Proverbio, E. Electrochemical behavior of hydrophobic silane–zeolite coatings for corrosion protection of aluminum substrate. *J. Coat. Technol. Res.* **2014**, *11*, 883–898. [[CrossRef](#)]
34. Lyon, S.B. Corrosion of tungsten and its alloys. *Shreir's Corros.* **2010**, *3*, 2151–2156.
35. Hirschorn, B.; Orazem, M.E.; Tribollet, B.; Vivier, V.; Frateur, I.; Musiani, M. Determination of effective capacitance and film thickness from constant-phase-element parameters. *Electrochim. Acta* **2010**, *55*, 6218–6227. [[CrossRef](#)]
36. Brug, G.J.; van den Eeden, A.L.; Sluyters-Rehbach, M.; Sluyters, J.H. The analysis of electrode impedances complicated by the presence of a constant phase element. *Electroanal. Chem.* **1984**, *176*, 275–295. [[CrossRef](#)]
37. Sebastian, D.; Yao, C.; Lian, I. Mechanical durability of engineered superhydrophobic surfaces for anti-corrosion. *Coatings* **2018**, *8*, 162. [[CrossRef](#)]
38. Sun, R.D.; Nakajima, A.; Fujishima, A.; Watanabe, T.; Hashimoto, K. Photoinduced surface wettability conversion of ZnO and TiO<sub>2</sub> thin films. *J. Phys. Chem. B* **2001**, *105*, 1984–1990. [[CrossRef](#)]
39. Rahimi, E.; Rafsanjani-Abbasi, A.; Kiani-Rashid, A.; Jafari, H.; Davoodi, A. Morphology modification of electrodeposited superhydrophobic nickel coating for enhanced corrosion performance studied by AFM, SEM-EDS and electrochemical measurements. *Colloids Surf. A Physicochem. Eng. Asp.* **2018**, *547*, 81–94. [[CrossRef](#)]
40. Khorsand, S.; Raeissi, K.; Ashrafizadeh, F.; Arenas, M.A. Super-hydrophobic nickel–cobalt alloy coating with micro-nano flower-like structure. *Chem. Eng. J.* **2015**, *273*, 638–646. [[CrossRef](#)]
41. Cassie, A.B.D.; Baxter, S. Wettability of porous surfaces. *Trans. Faraday Soc.* **1944**, *40*, 546–551. [[CrossRef](#)]